To appear in the Newman Honorary Volume of the Journal of Engineering Mathematics (2007)

Weak or strong nonlinearity: the vital issue

R.C.T. RAINEY

Atkins Ltd., Oil & Gas Division, Euston Tower, 286 Euston Road, London NW1 3AT, U.K.
(E-mail: rod.rainey@atkinsglobal.com)

Abstract. Marine hydrodynamics is characterised by both weak nonlinearities, as seen for example in drift forces, and strong nonlinearities, as seen for example in wave breaking. In many cases their relative importance is still a controversial matter. The phenomenon of particle escape, seen in linear theory, appears to offer a guide to when strongly nonlinear effects will start to become important, and what will happen when they do.

In the case of the "ringing" of vertical cylinders in steep waves, particle escape is shown to correspond approximately to local wave breaking, which leads to the cavitation responsible for "ringing". Another example is rogue waves, where recent results from weakly-nonlinear theory are disappointing, and also fail to explain the rogue waves seen in relatively shallow water, as in the data from the Draupner and Gorm platforms. Recent laboratory experiments, too, show wave crests continuing to grow in height after all frequency components have come into phase, which is inconsistent with weakly nonlinear theory. Particle escape, which is more frequent in shallow water, offers a simple alternative explanation for these observations, as well as for the violent motion at the wave crests, which often confuses rogue wave data. Extreme wave crests have long been known to be strongly-nonlinear, so it appears possible that rogue waves are primarily a strongly-nonlinear phenomenon.

Fully-nonlinear computations of two interacting regular waves are presented, to explore further the connection between particle escape and wave breaking. They are combined with Monte-Carlo simulations of particle escape in hurricane conditions, and the very few measurements of large breaking waves during hurricanes. It is concluded that large breaking waves will have occurred about once per hour, and once per 100 hours, respectively, in the recent hurricanes LILI and IVAN. These findings call into question the use of non-breaking wave models in the design codes for fixed steel offshore structures.

Key Words: freak waves, hurricane damage, offshore structures, rogue waves, wave breaking

1. Introduction

It is a great pleasure to contribute to this Volume in honour of Nick Newman's 70th birthday. I have known him personally for 15 years, and twice that time by reputation. I can certainly concur with John Grue's observation in his introduction to the Proceedings of the 20th IWWWFB [1], that Nick Newman has been the world's foremost expert in the field of marine hydrodynamics, for more than a generation. I would also concur with Finn Gunnar Nielsen's remark in the same introduction, that his personal qualities, especially his kindness, and his respect and tolerance for all, has perhaps been equally important, as a lesson in the way that the international research community should behave. His modest reply to his birthday speeches at the 20th IWWWFB sufficiently illustrate this point. Nick said that we should not believe a word of the praises just heaped upon him, and that he wished the Anglo-Saxons would show a greater appreciation to the rest of the world, for being prepared to speak English at international meetings! This is a civilised voice indeed, reminiscent of Henry Thoreau (an earlier voice from Massachusetts), and Mark Twain.

I would like to use this opportunity to address what I believe to be one of the fundamental characteristics of marine hydrodynamics, and one of the main reasons for its continuing vitality. This is that it has two types of nonlinearity: weak and strong. The importance of this distinction was first highlighted, to my knowledge, by M.S. Longuet-Higgins. Weak nonlinearity is seen for example in wave drift forces, which are the nonlinear effect whereby waves generate steady forces on floating bodies. Wave drift forces are typically proportional to the square of the wave height, and can be analysed with a perturbation scheme (Stokes' expansion), taken to second order in wave steepness, as of course in Newman's approximation. Strong nonlinearity is seen most obviously in wave breaking, and in related wave impact effects. These cannot be analysed by the Stokes perturbation scheme, as is conclusively shown by the fact that the water surface overturns, and cannot therefore be described as a Fourier series.

I would like to deal with three examples where the relative importance of weak and strong nonlinearity is not clear, and where the issue is still (or has recently been) controversial:

1. "Ringing" of vertical cylinders in steep waves. This is a transient high-frequency structural vibration, discovered during the design of large concrete oil rigs in Norway in the 1990s. It is produced when steep waves interact with an elastically-mounted vertical cylinder, of diameter comparable with the wave height, and natural period 10-30% of the wave period. Because the vibration can be in the region of the 3rd harmonic of the wave frequency, 3rd order weakly nonlinear theory was developed, with considerable skill, to analyse the problem. However, high-speed photography revealed that the phenomenon is strongly nonlinear, and that the rapid loading cycle causing the "ringing" vibration is traceable to local wave breaking around the cylinder, leading to cavitation behind it.

2. Rogue waves. Weakly nonlinear theory shows that regular waves are unstable, and degenerate into wave groups. In the right circumstances, these groups can continue to self-focus into large isolated waves, up to 3 times higher than the original regular waves. This has been widely suggested as the explanation for rogue waves. Recent computations suggest that this type of self-focusing is not statistically significant in irregular waves, however. I will discuss new evidence which points in the same direction, and suggests that strong nonlinearities may better explain the observed anomalies in wave data. This is a controversial view.

3. Wave breaking. Large-scale wave breaking is unusual in deep water, but is of great engineering importance when it does occur, because of the damage it can cause. The mechanism responsible for wave breaking is unclear - again, it has long been suggested that the weakly nonlinear instabilities of regular waves may be relevant, because they can ultimately lead to breaking. However, I will discuss a strongly nonlinear explanation, which appears to be useful in making quantitative predictions of breaking statistics. It also calls into question the widespread use of non-breaking wave models, in the design codes for offshore structures. This is again a controversial view.

In all three cases I will demonstrate that a useful indicator of when strongly-nonlinear behaviour begins, and what form it will take, is particle "escape". This is a phenomenon seen for example when two first-order regular waves interact, and is illustrated in Figure 1, which shows two such waves of 2:1 length ratio.

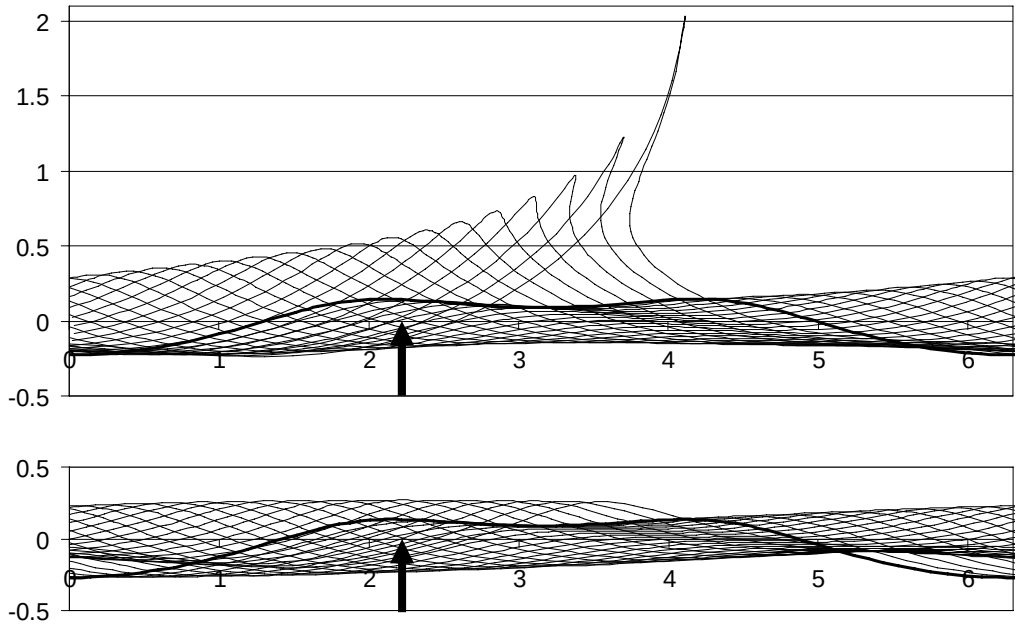

Figure 1. The upper graphs are successive positions of a sheet of particles initially on the zero-pressure surface, for two 1st order waves of the same steepness ka = 0.18, one twice the length of the other. The lower graphs are the corresponding conventionally-defined surfaces (1.1). One wavelength of the longer wave (2π) is illustrated, and the vertical and horizontal scales are the same. The bold line is the initial position, when the crest of the longer wave, and the trough of the shorter wave, are both at π. Subsequent lines show the surface at successive time-steps equal to 5% of the time until the conventionally-defined crests coincide. The arrow shows where this crest coincidence occurs.

If their amplitudes, wavenumbers and frequencies are a_1, k_1, ω_1, and a_2, k_2, ω_2, the surface elevation is given by linear theory as:

$$a_1 \cos(k_1 x - \omega_1 t) + a_2 \cos(k_2 x - \omega_2 t) \tag{1.1}$$

where x is horizontal position and t is time, and we are taking $k_1 = 1$, $k_2 = 2$, and equal wave steepnesses of $k_1 a_1 = k_2 a_2 = 0.18$. At the bottom of Figure 1 this surface is shown at successive times starting from when the crests of the long wave coincide with the trough of the short wave, and continuing up to (and beyond) the point where the crests of the two waves coincide.

The top of Figure 1 shows the corresponding position of surface particles, which are tracked computationally as they move in the linear velocity field, defined by the velocity potential φ given by:

$$\frac{a_1 \omega_1}{k_1} e^{k_1 z} \sin(k_1 x - \omega_1 t) + \frac{a_2 \omega_2}{k_2} e^{k_2 z} \sin(k_2 x - \omega_2 t) \tag{1.2}$$

where z is vertical position measured upwards from the still water level, and we are assuming deep water so that $\omega_1^2 = k_1 g$ and $\omega_2^2 = k_2 g$ where g is the acceleration due to gravity.

The initial condition of the particles is that they are placed on the zero-pressure surface, where the pressure p is defined by the exact pressure formula:

$$p = -\rho g z - \rho \frac{\partial \varphi}{\partial t} - \frac{1}{2} \rho \nabla \varphi \cdot \nabla \varphi \tag{1.3}$$

where ρ is the water density, and the pressure datum $p = 0$ is atmospheric pressure. This initial surface can be seen in Figure 1 to be very similar to the conventional surface (1.1) – the small difference being a measure of the surface pressure error in linear theory. The particles thus define a surface which is a small improvement on linear theory in this respect – but only initially.

As can be seen in Figure 1, the sheet of particles overturns shortly after the crests of the two waves have coincided, and then the particles involved move violently upwards. The reason for this behaviour is readily seen from the simpler case of a regular wave, where we can make the flow steady by switching to a frame of reference moving with the wave crests. The streamlines in this frame are shown in Figure 2 below.

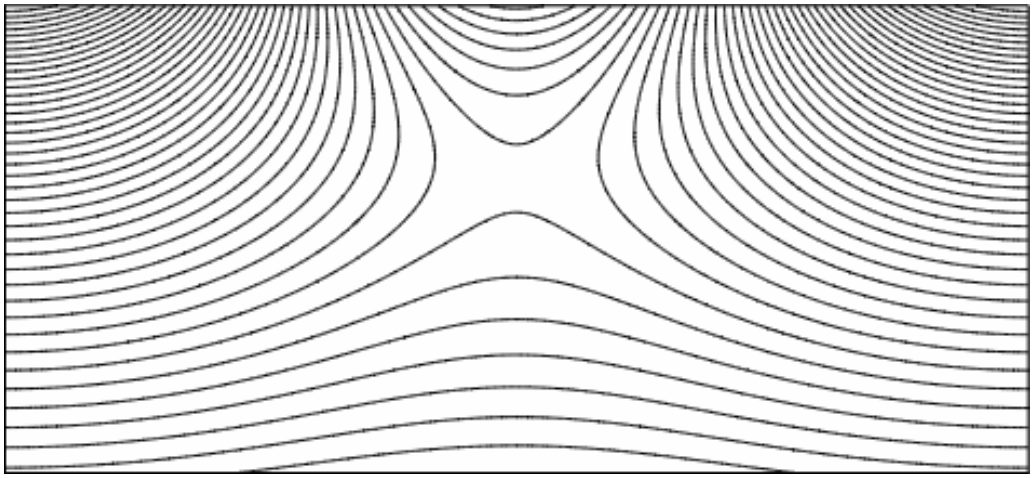

Figure 2. Streamlines in a regular wave, according to linear theory. The frame of reference is moving with the wave, so that the flow is steady. Vertical and horizontal scales are the same, and the horizontal axis covers one wavelength

The free surface in linear theory is a sinusoidal approximation to whichever of these streamlines most accurately satisfies the condition that the pressure (1.3) is zero. As waves of increasing steepness are considered, it is an increasingly-steep streamline. Eventually, the streamlines diverge from the wave crest. This is because the orbital velocity of the particles, when seen in a fixed frame of reference, has exceeded the speed of the wave. In the moving frame of Figure 2, therefore, the velocity is not merely reduced in the wave crest, but reversed. When the first diverging streamline is reached, the particles suddenly behave in a completely different manner, moving violently upwards, with ever-increasing velocity – in fact they escape to infinity in finite time, see Appendix. Similar behaviour is seen at the top of Figure 1, which we will henceforward refer to as a *particle escape*. We will see in Section 3 that it is in practice a very well-defined event, even in fully-irregular waves.

A particle escape means that the kinematic boundary condition, that surface particles remain on the surface, is no longer satisfied, even approximately, so that the errors in the linear theory,

which the higher order terms in Stokes' expansion are seeking to correct, are very large. See Stokes' original paper [2], which considers the kinematic error on the zero-pressure surface in a velocity field exactly like Figure 2, obtained by separation of variables and thus not restricted to $z < 0$. We might therefore expect that Stokes' expansion may diverge, and thus the weakly nonlinear theory be no longer valid. However, we can also readily see from Figure 2 that particle escape does not correspond exactly to the limit of validity of the weakly-nonlinear theory. This is because in this simple case of a regular wave, it is known [3] that the weakly nonlinear theory continues to be valid (with appropriate choice of the expansion parameter) up to the limiting regular wave with a 120-degree Stokes crest. This 120 degree crest is not seen in the dividing streamline in Figure 2, which instead forms a 90 degree crest.

Thus particle escape appears to be an indicator of the limit of validity of the weakly-nonlinear theory, but only an approximate one. In this paper we will explore how useful it is in practice.

2. "Ringing" of vertical cylinders in steep waves

The phenomenon of "ringing" was discovered in Norway in the 1990s, during model tests on the very large concrete oil rigs for the Heidrun and Draugen offshore oilfields. Bursts of high-frequency structural vibration were seen, coinciding with the passage of steep, but not breaking, waves. The phenomenon was unexpected (although as usual, earlier evidence of the phenomenon was soon discovered, in model test reports dating back to the 1970s, and even in full-scale measurements), and required late design changes to both rigs. Sophisticated computational techniques were rapidly developed to address the problem, notably an extension to 3rd order of the classical weakly nonlinear theory (i.e. Stokes' expansion) of wave diffraction around a vertical cylinder [4], and a simpler version of this theory [5] for the special case of long wavelength relative to cylinder diameter. Both relied on the observation that the vibration was not far from the 3rd harmonic of the wave frequency, suggesting that it may be a 3rd order weakly-nonlinear phenomenon.

However, careful model tests on vertical cylinders in these conditions showed [6] that there was a "secondary loading cycle", associated with violent motion of the water surface. In later experiments [7] it was shown by high-speed photography that there is local breaking around the cylinder, leading to the formation of a cavitation (or more strictly a ventilation) bubble behind it, which then collapses to give the secondary loading cycle. There is no connection with the 3rd harmonic of the wave frequency – the natural frequency of the cylinder can be set at much higher multiples of the wave frequency, and the "ringing" phenomenon persists, with the vibration envelope changing to follow the shape of the secondary loading cycle. It is a strongly-nonlinear phenomenon, like wave breaking.

Figure 3, taken from more recent experiments [8], shows high-speed photographs of the water surface during this secondary loading cycle, as observed during laboratory experiments, in the transient wave at the start of a regular wave train. In the absence of the cylinder, this wave is well short of breaking, and has a surface elevation time-history which is readily reproduced by linear theory, as the sum of just two frequency components. The corresponding linear diffracted waves around the cylinder are the well-known McCamy-Fuchs combination of Bessel functions, see e.g. [9, p.390]. As in Figure 1, particles were followed in this linear velocity field, starting from their position on the linear free surface at the null before the event illustrated. The surface defined by the subsequent position of this sheet of particles is shown in the second column of figures in Figure 3, and the final column shows comparative measurements of the surface position immediately adjacent to the cylinder.

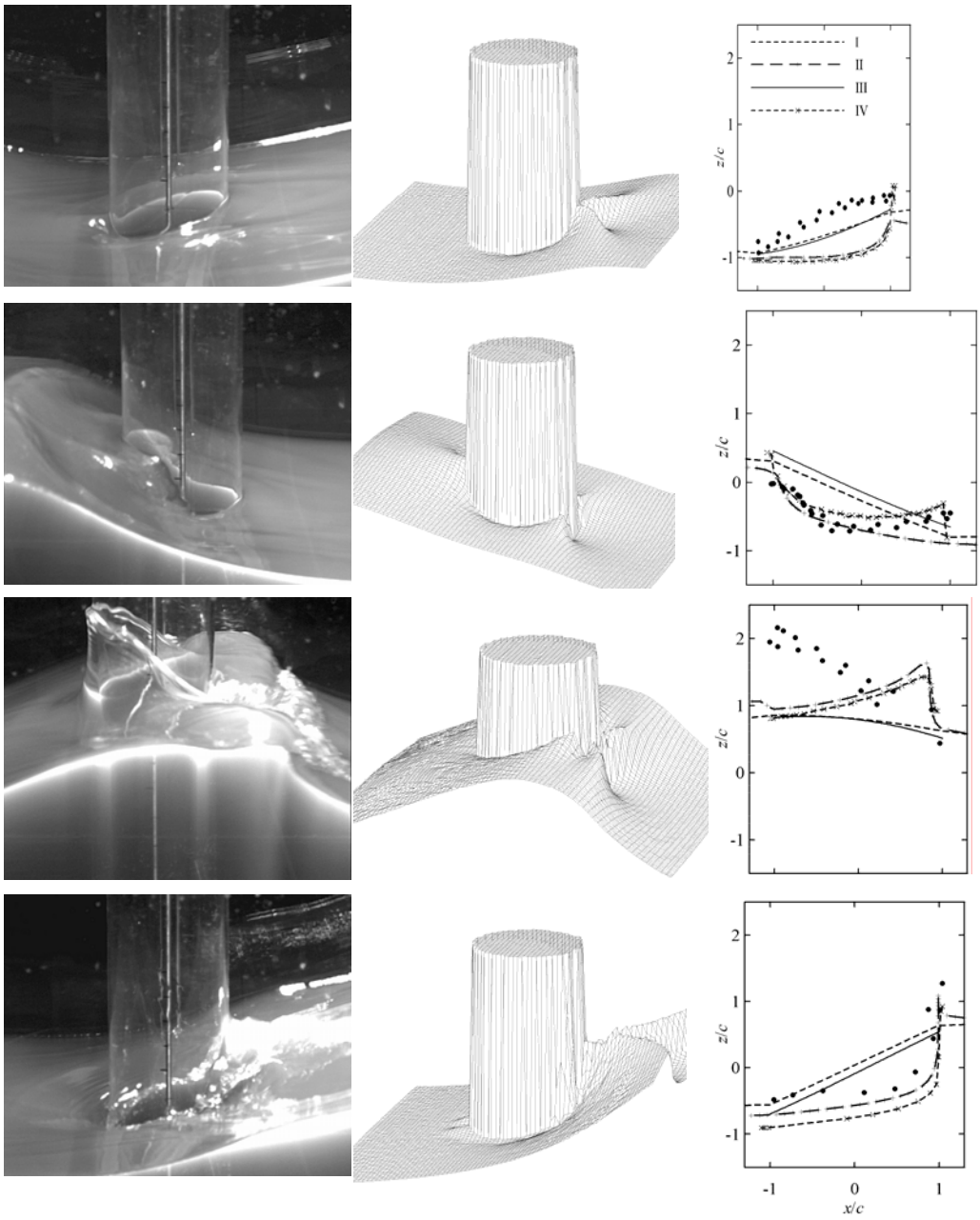

Figure 3. Laboratory observations (left column) and simulations (middle column) of the water surface, at intervals of 0.2s, around a cylinder of 10cm diameter, in a wave of 0.8s period. The simulations were obtained by following surface particles moving in the velocity field defined by the MacCamy-Fuchs linear potential. The viewing angle of the simulations is shifted by 15^{o} in yaw relative to that of the laboratory observations. The right column shows the corresponding water surface elevations alongside the cylinder in the simulations (IV), the .MacCamy-Fuchs linear free surface position as conventionally defined (III), and slender body approximations to both (II and I respectively). Measurements are shown as points.

The most striking result is that the breaking wave seen propagating around the cylinder between the second and third images, is also seen in the particle-sheet simulations, despite the fact that they only use linear theory. This local breaking is a strongly-nonlinear phenomenon, leading to the cavitation behind the cylinder seen in the third image, and the associated secondary loading cycle.

The behaviour of the surface particles moving in the linear velocity field, still short of particle escape, is evidently a good guide to the onset of strongly-nonlinear behaviour.

3. Rogue waves

The celebrated Benjamin-Feir instability of regular waves [10] is a weakly nonlinear effect (3rd order in Stokes' expansion) which has given rise to a whole branch of the theory of water waves, see e.g. [11]. This has been further stimulated by the discovery of exactly equivalent effects in nonlinear optics. Following Peregrine's discovery [12] that an ultimate weakly nonlinear evolution of regular waves was into a single wave about three times higher than the original regular wavetrain, it has been widely suggested (e.g. [13]) that weakly nonlinear theory might explain rogue waves, i.e. waves too big to be explained by Stokes 2nd order theory.

However, recent developments have not lent support for this view. The latest computations [14] show that the effect of this weakly nonlinear evolution on crest elevation statistics is negligible except when the initial wave spectrum is unrealistically narrow, and even then it is not large (~10% increase in extreme crest elevation seen in 10^4 waves, compared with 2nd order theory). Also, in one of the best-documented cases of a rogue wave, on the Draupner oil rig in 1995, where there was a wave crest elevation of 1.55 times the significant waveheight [15], it has been recently shown [16] that the water is too shallow for weakly nonlinear spectral evolution. This is essentially because the spectral peak in that wave is at 0.0633 Hz (see Figure 5 below) which corresponds to kd = 1.307 in the Draupner depth of d = 70m, whereas the Benjamin-Feir instability requires a minimum kd of 1.363 [10]. This is even more so in the depth of 40m at the Gorm oil rig, where there is a much more extensive collection of published data [17], including rogue waves with wave crest elevations up to 2.07 times the significant waveheight.

Strongly-nonlinear features, apart from breaking, have long been recognised in steep waves. See Figure 4, taken from [7], which shows the phase speeds of the frequency-components of a focused wave, as measured in the laboratory from the phase difference detected by a pair of closely-spaced wave probes. The mechanically generated waves, produced by the wave-maker, are in the range 0.511 – 1.244 Hz. All the other components arise naturally through nonlinear interactions. Well before focus, when the waves are still small, the phase speeds of these components can be seen (top of Figure 4) to be as predicted by weakly-nonlinear theory, i.e. at multiples and submultiples of the speed C_1 of a free-running linear wave. But close to focus, the high-frequency components all lock onto the same speed, so that for a short time the wave resembles a large regular wave. This is a strongly-nonlinear phenomenon, first described in [18], and confirmed by many subsequent workers, see papers cited in [7].

Of particular interest in the context of rogue waves is the observation [19, fig.3] that if the phases of the mechanically-generated waves are carefully adjusted to bring all these components exactly into phase at focus (compensating for the pronounced de-focusing caused by nonlinear changes in phase speed, which are of course another well-known weakly-nonlinear effect [20]), then all the naturally-occurring wave components come into phase too, apart from the low-frequency set-down, which is in anti-phase, as predicted by weakly-nonlinear theory. And yet the wave crest elevation may be seen to *continue to grow* thereafter [19, fig.6a], by

approximately 10% in the case studied there, where the wave was not steep enough to break. The growth is presumably [19, after fig.3] because the set-down ceases to be in anti-phase. A similar phase change of the set-down is revealed in [15] in the Draupner rogue wave, where its inconsistency with weakly-nonlinear theory is highlighted.

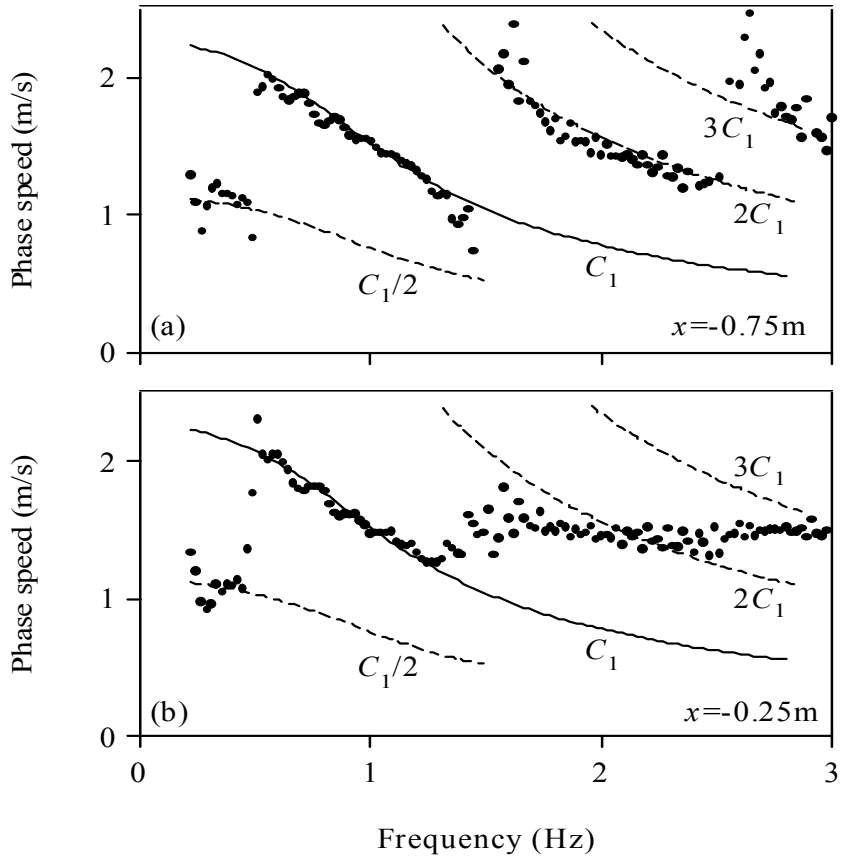

Figure 4. Measured phase speeds in a focused wave, near focus (below) and well before it (above). x is position in the direction of wave travel, from the focus point. Mean wavelength is about 1.7m.

This growth in crest elevation is reminiscent of the behaviour seen in Figure 1, in which the elevation of the crest particles grows without limit. In that case the dynamic boundary condition of zero pressure is being progressively violated, with the surface pressure becoming more and more negative, as if the surface were being sucked up. When the suction pressure is removed, it is plausible that the effect may remain, to some extent, and this is confirmed by the exact computations in the next Section (see Table 2). It is therefore pertinent to enquire whether the particle escape seen in Figure 1 occurs in the wave spectrum at the time of the Draupner rogue wave. This spectrum is given in Figure 5 below, taken from [15].

It is normal practice in rogue wave predictions (e.g. [13, 14]) to ignore the high-frequency tail of the spectrum. In figure 5, the natural choice for such a truncation-frequency is 0.094 Hz, where there is a pronounced drop in spectral density. There is also practically no energy below 0.047 Hz; in this way the spectrum is restricted to a convenient maximum-to-minimum frequency ratio of exactly 2. This truncation reduces the significant waveheight by 10%; the lost

waveheight was restored by scaling up the truncated spectrum so that the significant waveheight was 12m.

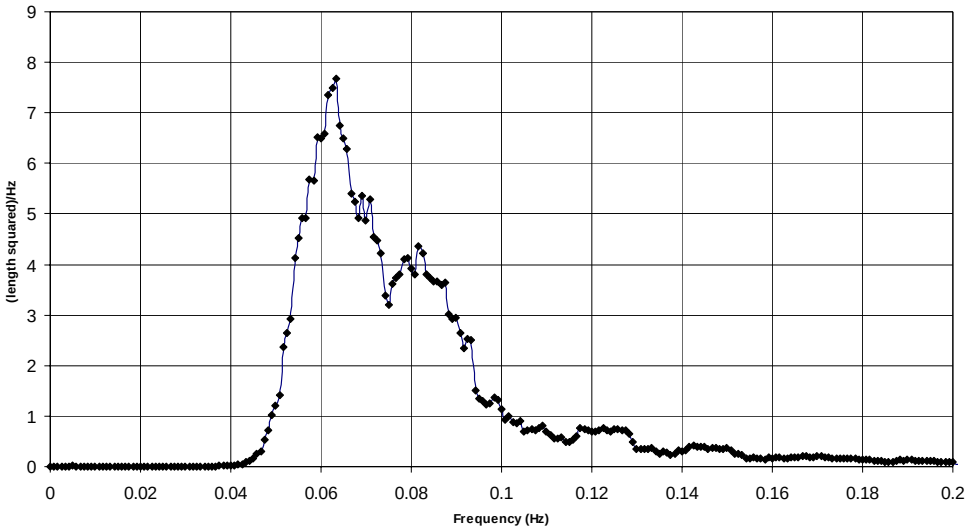

Figure 5. Measured wave spectrum at the time of the Draupner rogue wave, obtained from the 20-minute record containing the rogue wave. The peak is at 0.0633 Hz. The significant waveheight, defined at 4 times the standard deviation of the record, was 11.92m.

The linear velocity potential was then defined in the usual way as the sum of N components:

$$\sum_j \frac{\omega_j}{k_j}\sqrt{2S(\omega_j)\delta\omega}\,\frac{\cosh k_j(z+d)}{\sinh k_j d}\sin(k_j x-\omega_j t+\Phi_j) \tag{3.1}$$

where $S(\omega)$ is the wave spectrum of Figure 5 truncated as just described, and Φ_j are random phase angles. The infinite-depth form (1.2) of the velocity potential is now replaced by the finite-depth form, with the wavenumbers k_j given by $k_j g \tanh(k_j d) = \omega_j^2$. The N frequencies ω_j were chosen so that the corresponding wavnumbers k_j were equally spaced.

The occurrence of particle escapes can be investigated very simply, by tracking a single particle started at the zero-pressure surface as in Figure 1 (a refinement is to wait until this zero-pressure surface crosses zero, before starting), and then moving in the flow field defined by (3.1). A typical result obtained in this way is shown in Figure 6 below. The orbital motion of the particle is evident, as well as its steady Stokes drift in the downwave direction. After a number of wave cycles, however, the particle escapes violently upwards. The motion is so violent that it produces a numerical overflow – the particle appears to escape to infinity in finite time, as in the regular wave case, described in the Appendix. Accordingly, the particle is "trapped" by setting the velocity to zero after it reaches an elevation of 50m. The statistical results below are not visibly altered if this elevation is increased to 200m.

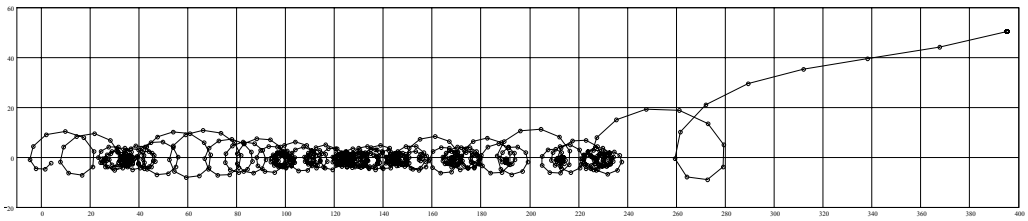

Figure 6. Trajectory of a particle initially on the zero-pressure surface, and moving thereafter in the velocity field (3.1), with the Draupner wave spectrum of Figure 5, truncated to give a maximum-to-minimum frequency ratio R of 2.00. The number N of spectral lines was 50. The vertical and horizontal scales are both in metres, and the particle escapes after about 20 minutes.

However, there are cases of the particles reaching a large elevation but not escaping; one such can be seen in Figure 6, where the particle reaches an elevation of nearly 20m. In 300 repeats of the simulation shown there, each 1 hour long, but with other choices of the random phase angles Φ_j there was only a single case of a particle escape, which is the one illustrated. In these 300 hours, there were 3 cases where the elevation reached 30m without escaping, but none where it exceeded 35m. It is arguable that if the particle elevation exceeds 30m, then the kinematic errors in linear theory are so large that Stokes' expansion is likely to diverge and give strongly-nonlinear behaviour. This could well be true (as in Figure 3, where strongly-nonlinear behaviour is occurring before particle escape) but the convenient datum is obviously particle escape, because it corresponds to the most extreme events, which are the ones of interest in the context of rogue waves.

To explore the frequency of particle escape, more extensive simulations are required. As can be seen in Figure 6, there is remarkably little drift of the particles in a vertical direction, in contrast to their large horizontal drift. This is a very convenient property, and arises because a whole sheet of surface particles cannot drift vertically in potential flow, unless there is loss of fluid volume under it, which in our case is prevented by the seabed (or the stationary deep water, in the infinite depth case). Beyond 100 hours, however, a slight downward drift can be clearly seen in long simulations, which biases the escapes towards the earlier part of the run. This may be simply a numerical limitation, or a slight loss of fluid volume caused by escapes elsewhere. It is immaterial in practice, because a few long simulations are no quicker than many shorter ones. Accordingly, the simulation length was chosen as 3.33 hours, so that a batch of 300 simulations corresponded to 1,000 hours. 25 such batches were then performed, giving 25,000 hours or about 10^7 waves. This is easily comparable with other recent work on rogue waves, for example [14] considers 10^4 waves over durations up to 100 wave periods.

The 25,000 hours were made up of 25×300 = 7500 simulations, in the great majority of which there was no particle escape. When one occurred, however, the waiting-time before the escape occurred, measured from the beginning of the simulation, was recorded. If the escapes are occurring at random, these waiting-times should fit the exponential distribution for the waiting-time in a Poisson process. We can therefore compare with this distribution, using a Q-Q plot, see e.g. [21, sect.10.2.3]. The waiting-times before particle "escape" are first sorted into ascending order, and then the nth waiting time is plotted against the corresponding nth 7500-quantile of the exponential distribution. If the mean waiting time is T, then the exponential distribution gives the cumulative distribution function for the waiting time t as:

$$1 - e^{-\frac{t}{T}} \tag{3.2}$$

Thus the nth 7500-quantile t_n is given by:

$$1 - e^{-\frac{t_n}{T}} = \frac{n - 0.5}{7500} \qquad \text{i.e.} \qquad t_n = T\left\{-\ln\left(1 - \frac{n - 0.5}{7500}\right)\right\} \tag{3.3}$$

We can therefore plot our sorted waiting-times against $-\ln\{1 - (n\text{-}0.5)/7500\}$. If they follow an exponential distribution, the result should be a straight line of slope equal to the mean waiting-time T. Figure 7 shows these plots, where the number of spectral lines N is taken as 50, 100 and 200, to check for numerical convergence. To reveal also the importance of the water depth of 70m at Draupner, all the simulations were repeated with the infinite-depth form (1.2) of the velocity potential (3.1), and these results are given as well in Figure 7.

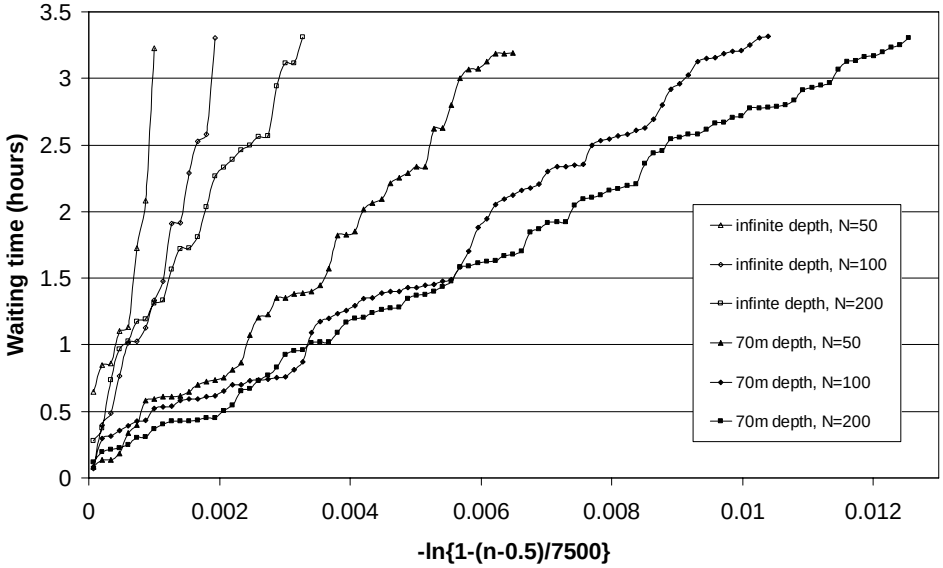

Figure 7. Waiting-times until a particle escape, from batches of 7500 simulations, plotted against $-\ln\{1 - (n\text{-}0.5)/7500\}$, where n is the position out of 7500 when sorted into ascending order. The spectrum was that shown in Figure 5, truncated to a maximum frequency ratio of 2, and scaled to a significant waveheight of 12m.

It can immediately be seen that the finite depth of 70m at Draupner is very significant, increasing the frequency of particle escapes by almost an order of magnitude. This is of course to be expected, from Figure 2, since in finite depth the horizontal particle velocities are increased, while the phase velocity is reduced. It can also be seen that the number N of spectral lines is important - however with the 70m depth, the results appear to have converged at N = 200. There is then a good fit to a straight line, implying escapes occurring at random, at a frequency of one every 3.2/0.012 = 270 hours.

This is consistent with the discovery of the Draupner rogue wave as a rare event among some years of wave data, with presumably hundreds of hours of storm conditions. It is also consistent with the greater numbers of more extreme events (up to crest elevations of 2.07 times significant waveheight [17], as already noted) seen in the Gorm data, where the water depth was only 40m. It suggests that the phenomenon of rogue waves may be largely explained as ordinary linear wave focusing, with the strongly-nonlinear consequences suggested by particle

escape. These strongly-nonlinear consequences are quick-acting, in contrast to the slow weakly-nonlinear evolution of extreme waves discussed at the start of this Section, so there should be no need for very long wave flumes to see them. A short wave flume, provided it has an efficient beach and an absorbing wavemaker so that it can be run for long periods without reflections building up, should be sufficient. It is merely necessary to repeat the numerical experiment of Figure 7 above. At a scale factor of 100:1, the 25,000 hours considered there would take 2,500 hours or about 3 months, which is just feasible. And the steeper seastates considered in the next Section would not need this long. See Figure 13, which suggests that 1,000 hours full-scale, or approximately 100 hours model scale, would be sufficient. It would also be possible to include wind in the experiments, because it is well-known (from the surfing and kayaking fraternity, and also in the technical literature [22, p.389]) to increase crest elevations when it blows in the opposite direction to the waves.

One feature of rogue waves that might be confirmed in this way, with the aid of high-speed photography, is that the crest can sometimes be thrown violently upwards in a jet, in the manner suggested by Figure 1. The phenomenon is readily observed at sea in the locally-extreme conditions produced when wind waves are augmented by ship waves. See Figure 8 below. Similar observations of violent jets at wave crests have recently been made in the laboratory, in focused waves [23].

Figure 8. Interaction between waves generated by a boat, and local wind waves of approximately half the length. Note violent upward motion of particles in the crest, shown circled. Taken by the author from the *Dale Princess* (approx 15m long), off Skomer Island, Pembrokeshire, UK. The wind is blowing off the shore, in the direction that the boat is travelling, so that the wind-generated waves are at approximately 45 degrees to the direction of the ship waves.

This would neatly explain a recurrent theme of the rogue wave literature, which is that many of the physical measurements of crest elevations are disputed. The data from the Gorm field [17] cited above, for example, has be analysed elsewhere [24] with very different conclusions – the extreme crest elevations given in [24] are only about 1.6 times the significant waveheight, rather than 2.07 times it. This problem has been highlighted in the literature [25] where the problem is described as "spurious crests due to spray". A noteworthy recent example is the freak wave recorded on the North Alwyn platform [26, fig.1] which had a crest elevation 2.35 times the significant waveheight (which was 5.93m, based on the standard deviation of the record), but the crest appears as a pronounced "spike" in the time-history, capable of various interpretations.

4. Large-scale wave breaking.

After extreme crest elevations, the next most important wave parameter to offshore structures is the likelihood of large-scale wave breaking. Such events are not recorded by wave buoys (which in practice smooth out wave breaking, for a variety of reasons), but are seen in measurements from fixed gauges. A well-known published example is the large breaking wave seen during hurricane CAMILLE, which has been highlighted by several authors, e.g. [27, fig. 8.1, 28, fig.8], and is reproduced in Figure 9 below.

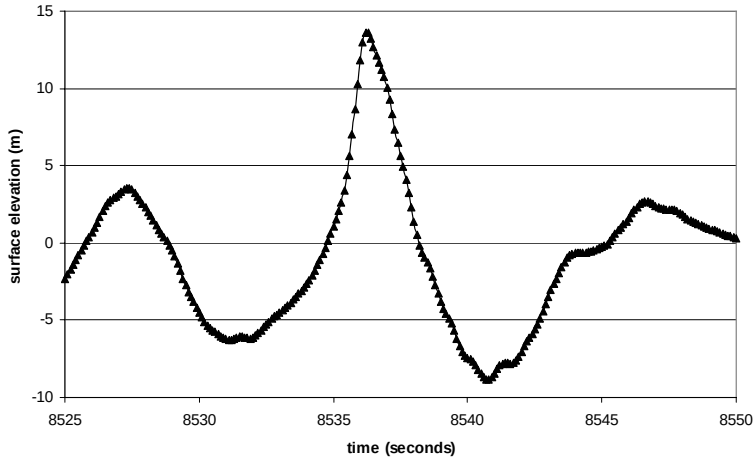

Figure 9. Large-scale breaking wave during hurricane CAMILLE, as recorded by a fixed wave staff. These measurements are published by the Ship Hydrodynamics Directorate of the U.S. Naval Surface Warfare Center, Carderock Division. Details are in [29]. The data shown, which has a sampling rate of 10 Hz, is taken directly from the Camille_1713C file, preserving the time recording used there, viz. seconds after 1300 hrs on 17th August 1969. The mean water level over the 1 hour duration of the record is -0.990m.

On the front face of this wave, the rate of increase in surface elevation is sustained at over 15 m/s, for nearly half the crest elevation. This is about the same as its phase speed, implying that the front face has a slope of 45 degrees, over a similar distance. Since the pressure is zero at the water surface (the dynamic free surface condition), the pressure gradient, which is the vector sum of particle acceleration and *g*, must be normal to the water surface. Thus when the surface slope is 45 degrees, the particle acceleration must be about *g*, which is much greater than the particle acceleration in a non-breaking wave, and will produce much larger wave loads, especially on large-diameter structural members.

What is required from an engineering point of view is some method of predicting the likelihood of a large breaking wave of this type, based on the readily available wave data, which is the wave spectrum as measured by wave buoys. To take a topical example, the spectra of all recent hurricanes in the Gulf of Mexico are measured by wave buoys operated by the US National Oceanic and Atmospheric Administration, and put into the public domain. The two most recent important hurricanes featured there are IVAN and LILI, whose spectra are shown in Figure 10 below, together with that of hurricane CAMILLE. An important parameter in these spectra is the *significant steepness*, i.e. the significant waveheight divided by the wavelength of the peak frequency of the spectrum (it is not to be confused with significant acceleration, i.e. twice the root-mean-square acceleration. This is very poorly defined, as explained below). This comes to 0.037, 0.043 and 0.041 respectively for IVAN, LILI and CAMILLE. These values are considerably higher than average seastates – the well-known Pierson-Moskowitz spectrum, for example, has a significant steepness of 0.025. They are however not exclusively associated with tropical hurricanes – pooled data from 1973-2001 from the North Sea shows [14, fig.2] a maximum significant steepness of about 0.055.

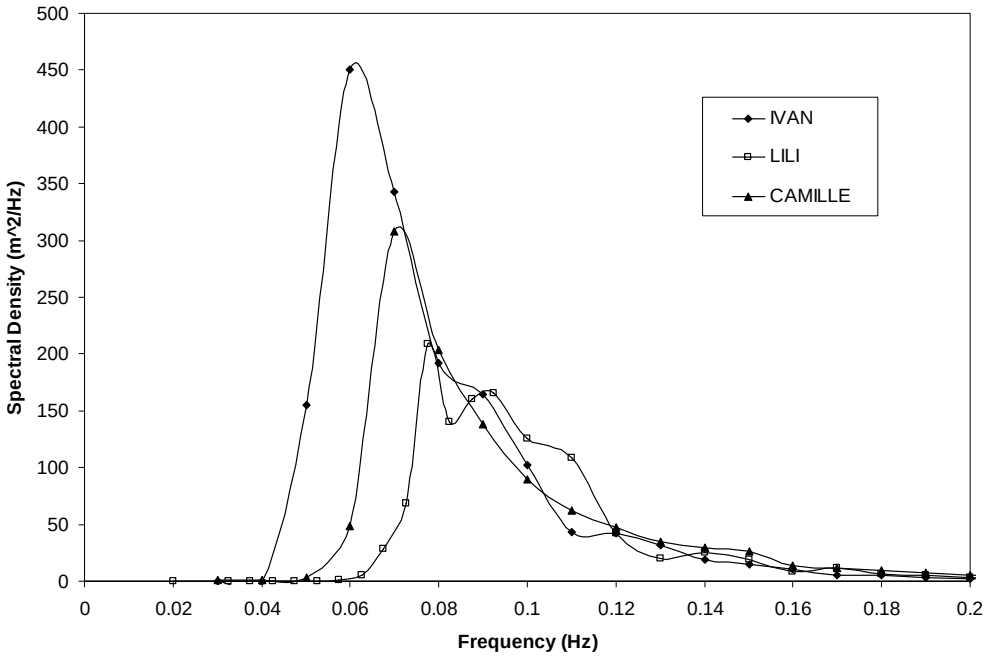

Figure 10. Measured wave spectra in hurricanes IVAN, LILI and CAMILLE. In the first two cases the spectra are taken from the U.S. National Data Buoy Center website www.ndbc.noaa.gov, for Buoy Station 42040 at 00.00hrs on 16th September 2004, and Buoy Station 42001 at 21.00hrs on 2nd October 2002, respectively. The significant wave heights, obtained from the areas under these spectra, are 16.0m and 11.2m, and the water depths are 444m and 3,246m, respectively. The CAMILLE spectrum shown is obtained from an FFT of the Camille_1713C file (see Figure 9) covering approximately the period from 1500hrs to 1600hrs, on 17th August 1969. The significant wave height, obtained from the variance of the data, is 13.1m, and the water depth is 100m.

The present state-of-the-art in predicting wave breaking is reviewed in [22] where it explained that the frequency of breaking is believed to be related to the frequency of exceedance (based on a linear prediction of the root-mean-square acceleration, and the Rayleigh distribution) of a given threshold of vertical particle acceleration. It is explained that the value

of this threshold is not well understood, and that values of 0.5*g* (i.e. the particle acceleration in the 120 degree Stokes crest) and 0.388*g* (i.e. the particle acceleration in the most energetic regular wave) have been proposed, see [30] and [31] respectively. The frequency of wave breaking calculated in this way is shown in Table 1 below, for the three spectra of Figure 10.

	Whole Spectrum up to recorded limit of 0.4 Hz (= 10m wavelength)		Spectrum truncated to limit bandwidth to 3:1 frequency ratio		Spectrum truncated to limit bandwidth to 2:1 frequency ratio	
	0.388*g*	0.5*g*	0.388*g*	0.5*g*	0.388*g*	0.5*g*
IVAN	21	154	2,050	316,000	696,000	5.04×10^9
LILI	7	25	82	1,500	1,660	223,000
CAMILLE	5	16	157	4,410	15,600	9,180,000

Table 1. Average number of waves needed to exceed given acceleration thresholds once, from the Rayleigh distribution and the root-mean-square acceleration given by (4.1).

It can be seen that there is a very large variation in the results, depending on the way that the wave spectrum is truncated during the calculation of the root-mean-square vertical acceleration. This calculation uses the transfer-function between wave elevation and vertical acceleration, which is simply ω^2 irrespective of the water depth, so as to give the root-mean-square acceleration as the square root of:

$$\int_0^\infty \left[\omega^2\right]^2 S(\omega)d\omega \tag{4.1}$$

The well-known problem is that this integral is very sensitive to the high-frequency tail of $S(\omega)$, because of the ω^4 weighting. In particular, standard semi-empirical spectra such as the Pierson-Moskowitz spectrum have a ω^{-5} high-frequency tail, so the integral (4.1) does not converge as the upper limit tends to ∞, but gives a result which can be made as large as we please, by choosing a sufficiently large limit. Hence the very large variations with truncation frequency seen in Table 1. These can be interpreted as showing the length-scale of the breaking: the lower the truncation-frequency, the larger the scale of the breaking being predicted. However, given this inconclusive evidence, some people have argued that large-scale breaking does not occur at all on deep water [22, p.373].

It was argued by the author [32] that particle escape gave a simple insight into wave breaking, because of the overturning of the surface seen in Figure 1, which resembles breaking. This explanation of wave breaking was contrasted by the author [32, sect 6] with the alternative explanation that breaking is caused by an instability. The crest instability described by Longuet-Higgins and Tanaka [33] is the most relevant to breaking. Like the Benjamin-Feir instability described in the previous Section, it develops from a regular wavetrain, and is weakly nonlinear (being a small perturbation from a weakly nonlinear wave), but it is a superharmonic rather than

a subharmonic instability (i.e. all wave crests are affected equally, rather than some growing at the expense of others). However, it only occurs in regular waves with crests close to the 120 degree limiting form (waves with $ka > 0.429$, see [34, p.33]), its scale is small (only a few percent of the crest height is affected [34, fig.9]), and its growth rate is slow (about 1 wave period before breaking [34, fig.9]). In large-scale wave breaking the 120 degree limiting wave form is by-passed – indeed the extent to which it is by-passed is a measure of the total dimensions of the overturning [35, p.378].

The explanation of particle escape applies to large-scale breaking, and will now be explored quantitatively. The problem of wave breaking is evidently a longstanding and difficult one, yet of great engineering importance. Any additional evidence of large-scale breaking is therefore of interest, however modest.

We can first repeat the particle-sheet computations at the top of Figure 1 with an exact fully-nonlinear computer program, in which the velocity potential is continuously changed to keep the pressure at the surface particles zero. A particularly well-developed program [36, 37], based on the boundary integral method introduced by Longuet-Higgins and Cokelet [38], has been made available to the author. The case in Figure 1, of two linear waves of 2:1 wavelength ratio, is studied. For initial conditions, the program uses the same zero-pressure initial surface position defined there, together with the velocity potential on this surface, given by (1.2).

The results are shown at the top of Figure 11 below, for the cases where the steepness ka of each of the two waves ranges from 0.15 to 0.23, in steps of 0.01. In each case the wave either remains smooth-crested, or breaks – there is no mistaking the latter case, because a jet forms, which eventually stops the program (ideally when it touches the surface of the wave under it, but in practice somewhat before this). For each run, the wave is only shown once, at the furthest stage into breaking that the program could reach – three different resolutions were used (84, 167 and 251 computational points) were used, which gave identical results but stopped running at slightly different stages into breaking. If the wave did not break, the wave is shown instead at the stage of maximum crest elevation. Evidently the threshold for wave breaking is $ka = 0.19$. The equivalent particle-sheet simulations, in the style of Figure 1, are shown below this in Figure 11, where it can be seen that the threshold for particle escape is $ka = 0.17$. Evidently particle escape is quite a good guide to wave breaking, in this case.

It is also of interest to include in the starting conditions the 2nd order potential from the weakly nonlinear theory [39]. For the case of the 1st order potential (1.2) it is (assuming $k_2 > k_1$):

$$-a_1 a_2 \omega_2 e^{(k_2-k_1)z} \sin\{(k_2-k_1)x-(\omega_2-\omega_1)t\} \tag{4.2}$$

The fully-nonlinear computations of Figure 11 were therefore repeated with this 2nd order potential (4.2) included in both the calculation of the initial surface position (to have zero pressure), and in the potential on it. The results are shown in Figure 12 below – it can be seen that the threshold for wave breaking only changes slightly to $ka = 0.18$. It is also possible to include the 2nd order potential in the particle-sheet simulations, although this becomes increasingly questionable after a particle escape in the 1st order potential (i.e. in the equivalent case at the bottom of Figure 11), because then it is arguable that Stokes' expansion may have diverged, as described in Section 1. They are nevertheless included (both in the calculation of the initial surface position, and in the velocity field thereafter) at the bottom of Figure 12. It can be seen that the threshold for particle escape is delayed from $ka = 0.17$ in Figure 11, to $ka = 0.21$ in Figure 12.

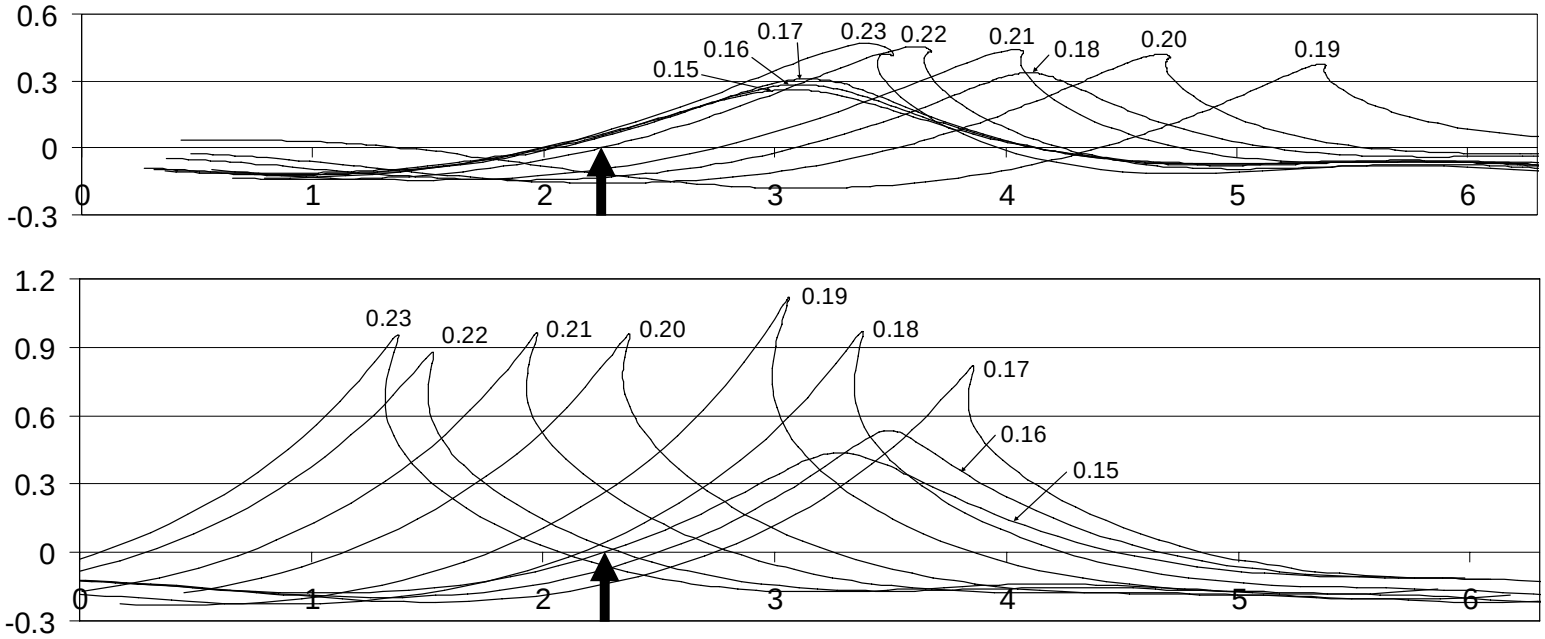

Figure 11. The upper graphs are the final positions of an exactly computed free surface, started at the zero-pressure surface in two 1st order waves, each of the same steepness *ka,* and with the crest of the long wave coinciding with the trough of the short wave. The graphs are labelled according to the value of *ka*. If there is no breaking, the highest position of the wave crest is shown instead of the breaking. The lower graphs are the equivalent positions of sheets of particles started in the same way, but moving in the classical 1st order flow. One wavelength of the longer wave (2π) is illustrated, and the vertical and horizontal scales are the same. The arrow shows where the classically-defined sinusoidal crests of the two waves coincide. See Figure 1 for the previous history of the wave, in the case $ka = 0.18$.

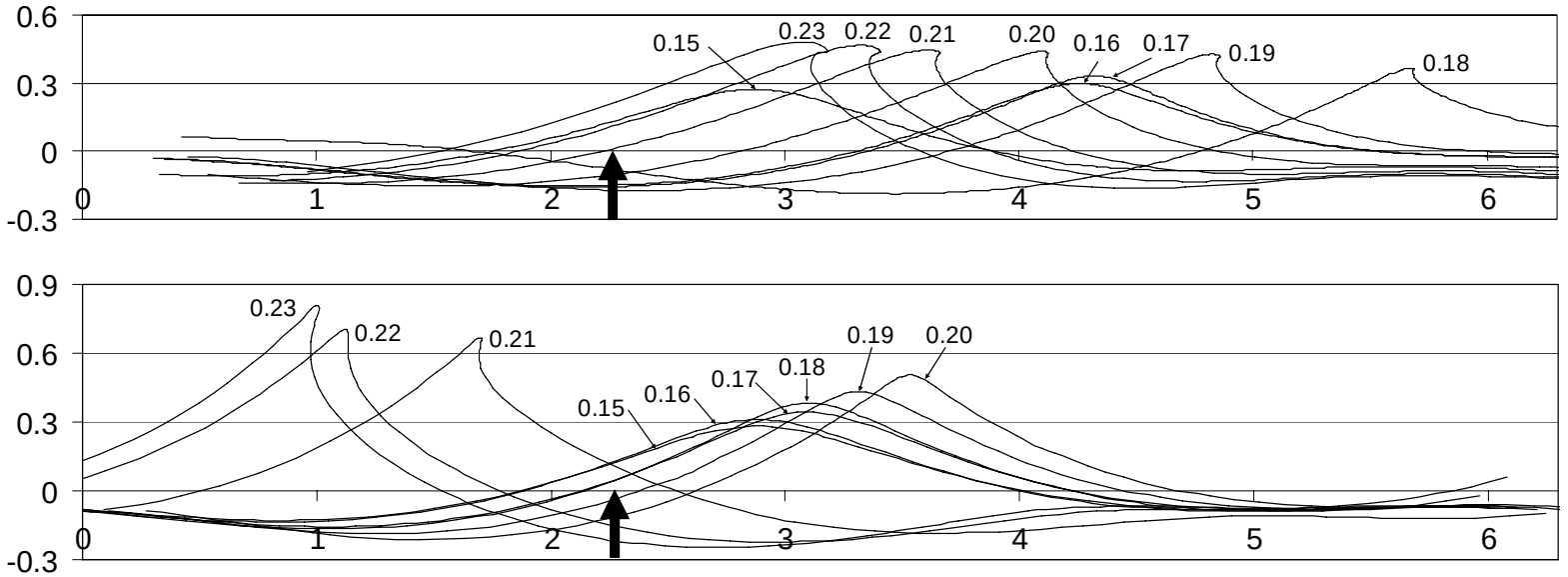

Figure 12. The upper graphs are the final positions of an exactly computed free surface, started at the zero-pressure surface in two 2nd order waves, each of the same steepness *ka,* and with the crest of the long wave coinciding with the trough of the short wave. The graphs are labelled according to the value of *ka*. If there is no breaking, the highest position of the wave crest is shown instead of the breaking. The lower graphs are the equivalent positions of sheets of particles started in the same way, but moving in the classical 2nd order flow. One wavelength of the longer wave (2π) is illustrated, and the vertical and horizontal scales are the same. The arrow shows where the classically-defined sinusoidal crests of the two waves coincide.

Figures 11 and 12 only show the exactly-computed waves at the end of the simulations. Since the crest elevation drops slightly as breaking progresses, we record also the maximum crest elevation reached in the computations, because of its relevance to the previous Section. See Table 2 below.

ka	Classical 2nd order theory (eqn. (4.4))	Exact computations	
		1st order starting conditions (Figure 11)	2nd order starting conditions (Figure 12)
0.15	0.253	0.261	0.271
0.16	0.272	0.284	0.297
0.17	0.291	0.308	0.331
0.18	0.311	0.336	0.375
0.19	0.330	0.377	0.428
0.20	0.350	0.421	0.439
0.21	0.370	0.439	0.450
0.22	0.391	0.458	0.473
0.23	0.411	0.475	0.484

Table 2. The maximum crest elevation in the exact computations of Figure 11 and 12, compared with the maximum crest elevation from classical 2nd order theory (4.4).

Also shown in the Table are the maximum crest elevations according to classical 2nd order theory, according to which the surface elevation is (see [35], but here we assume as in (4.2) that $k_2 > k_1$):

$$\begin{aligned} &\tfrac{1}{2}k_1{a_1}^2\cos 2(k_1x-\omega_1t)+\tfrac{1}{2}k_2{a_2}^2\cos 2(k_2x-\omega_2t)\\ &+\tfrac{1}{2}a_1a_2(k_1+k_2)\cos\{(k_1+k_2)x-(\omega_1+\omega_2)t\}\\ &+\tfrac{1}{2}a_1a_2(k_1-k_2)\cos\{(k_1-k_2)x-(\omega_1-\omega_2)t\} \end{aligned} \qquad (4.3)$$

Since in our case $k_1 = 1$ and $k_2 = 2$, and $k_1a_1 = k_2a_2 = ka$, the crest elevation when the two crests coincide ($x = t = 0$) is:

$$ka+\frac{ka}{2}+\frac{(ka)^2}{2}+\frac{(ka)^2}{4}+\frac{3(ka)^2}{4}-\frac{(ka)^2}{4}=\frac{3ka}{2}+\frac{5(ka)^2}{4} \qquad (4.4)$$

There is evidently a significant increase in crest elevation, when the wave breaks, compared with classical 2nd order theory. At $ka = 0.20$, for example, the crest elevation reaches 0.439 with the 2nd order starting conditions, compared with 0.350 from classical 2nd order theory. This is a 25% increase, which is significantly greater than the 10% increase reported in [14] with weakly nonlinear theory, and supports the view expressed in Section 3 that rogue waves may be largely a strongly-nonlinear phenomenon.

Returning to the correlation between particle escape and wave breaking, the case of a very low frequency ratio can be dealt without the need for computations like those in Figures 11 and 12. This is because the long wave groups involved are close to regular waves, where the thresholds for particle escape can be found from the streamlines in Figure 2. When the wave steepness is sufficient for the zero-pressure surface to reach the first diverging streamline, the

particles will begin to escape. This point is easily found – it is a 1st order wave steepness *ka* of 0.382. This is remarkably close to the experimentally-observed threshold of breaking of long wave groups, which is about *ka* = 0.38 [40 p.115].

No doubt this agreement is fortuitously close, but it is remarkable that the divergence of the streamlines in Figure 2, although long been recognised, has hitherto been considered to have no physical significance, see [41, 42] and also [32, written discussion by Tuck]. The closest suggestion in the literature, known to the author, is that when a Gerstner wave [43, art. 251] is modified to include a sloping sea bed, its jet-like limiting form should be taken as the shape of a breaker [44]. This is a fundamentally different phenomenon, because in a Gerstner wave the particles never escape, but move in closed orbits. The suggestion that the Gerstner jet corresponds to breaking, which was actually originally made by Gerstner himself (in his original paper [45], he says his jet occurs when *das Wasser an den Gipfeln der Wellen sich kräuselt*), has not been repeated in the more recent applications of the Gerstner idea (e.g. [46]), perhaps because the flow in the jet is so rotational – at the tip the vorticity is infinite, and thus the flow is completely unphysical. Also the Gerstner jet occurs at a height-length ratio of π^{-1} = 0.318, which is well above the experimentally-observed breaking threshold *ka* = 0.38 for long wave groups cited above, which corresponds to a height-length ratio of about $0.38/\pi = 0.12$.

We turn now to the correlation between particle escape and wave breaking in the case of two waves of high frequency ratio. Whatever the amplitude of the two waves, it is clear that a particle escape can be produced by sufficiently increasing the wavenumber k_2 of the short wave, because of the exponential term e^{kz} in (1.2). For the same reason, it has long been recognised in the engineering literature that classical linear wave theory is inadequate, and a rough-and-ready approximation ("Wheeler stretching" [47]) is used to suppress the exponential term. The phenomenon is also recognised in the mathematical literature, where at high ratios there are "short wave riding on long wave" models [48, 49, 50] in which the short wave is transported onto the surface of the long one, and responds to the "effective *g*" on its surface. Formally [51], if we write the 2nd order potential (4.2) in the form:

$$-a_1 a_2 \omega_2 e^{(k_2-k_1)z}\{\sin(k_2x-\omega_2t)\cos(k_1x-\omega_1t)-\cos(k_2x-\omega_2t)\sin(k_1x-\omega_1t)\} \quad (4.5)$$

we see that the first term in the brackets {} produces no phase change in the 1st order short-wave potential, and the second term produces a phase change which can never exceed 90 degrees. But the changes in wavelength of the short wave, as it responds to the changes in "effective *g*" on the surface of the long wave, will produce a cumulative phase change of the short wave (over a quarter-wavelength of the long wave, say), which can be made as large as we please, by making the wavelength ratio k_2/k_1 sufficiently large, and also keeping sufficient steepness k_1a_1 in the long wave. We can conclude [51] that Stokes' expansion must diverge, and thus the weakly nonlinear theory must break down.

It is not clear, however, whether the waves will break. Presumably if the wavelength ratio is sufficiently large, but the steepness of the two waves is sufficiently small, then there can be a particle escape (and an associated breakdown of the weakly nonlinear theory) but no wave breaking. It is therefore necessary to truncate the wave spectrum to exclude these cases, and more generally to exclude cases of small-scale breaking which are not of engineering importance. The situation is therefore exactly the same as with the acceleration-threshold breaking criterion of Table 1, except that a particle escape criterion is at least sensitive to water depth in a credible way, as shown in Figure 7.

Accordingly, we will truncate the hurricane spectra in Figure 10 to various degrees, and

investigate the frequency of particle escape in each case, just as in Table 1. The truncation can be achieved by working inwards from both zero and infinite frequency, until a certain threshold spectral density is reached. Only the main part of the spectrum, within these low and high-frequency limits, is then considered, as in Table 1. This was done for a range of threshold spectral densities, to obtain a range of truncated spectra from each of the three original spectra in Figure 10. The maximum-to-minimum frequency ratio R of these truncated spectra had various values, between 1.5 and 2.0. This captured approximately 85-90% of the significant waveheight, and thus significant steepness (no scaling of the truncated spectrum to restore the significant waveheight was performed, either here or in Table 1). The exact figures are given in Figure 13 below.

For each of these truncated spectra, a batch of 300 simulations totalling 1,000 hours was then performed, as in the previous Section. In these steeper seastates, a single batch of 300 simulations gave sufficient particle escapers to be statistically significant – it was not necessary to perform 7500 simulations. It was likewise sufficient this time to take the number N of spectral lines as 50 – some runs were repeated with N = 100, without giving significantly different results. The results for the LILI spectra are shown in Figure 13 below, in same Q-Q format as the previous Section (except that there are now 300 runs per batch, rather than 7500).

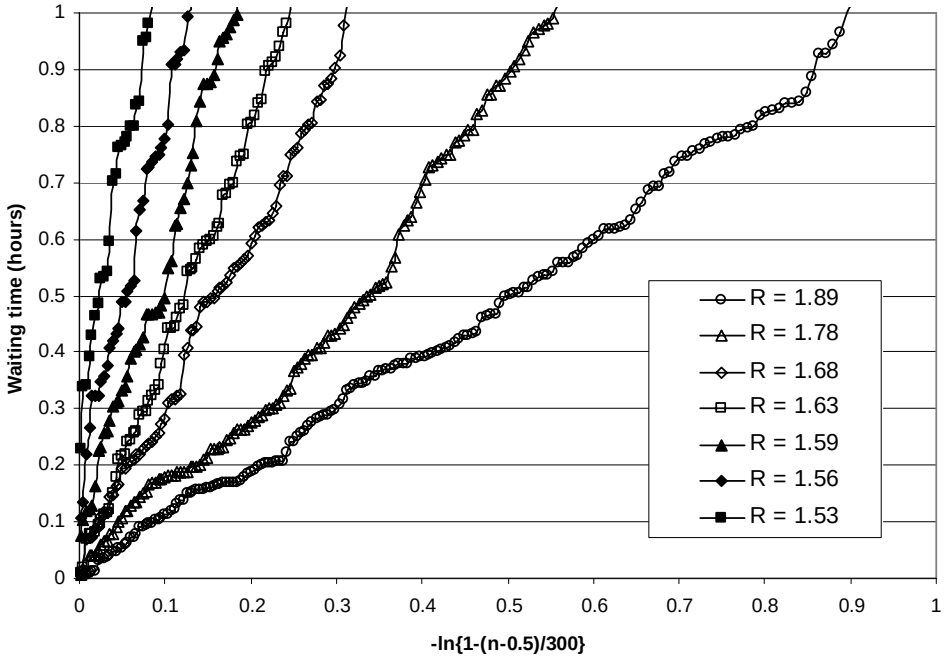

Figure 13. Hurricane LILI. Waiting-times until a particle "escape", from batches of 300 linear simulations, plotted against -ln{1 - (n-0.5)/300}, where n is the position out of 300 when sorted into ascending order. The parameter R is ratio of the maximum and minimum truncation frequencies applied to the LILI wave spectrum of Figure 10.

As in Figure 7, it can be seen that the Q-Q plots are close to straight lines, confirming that the escapes are occurring at random. A least-squares fit of the slope of the plots was accordingly made, to obtain the mean waiting times T. These are plotted, for all three hurricanes, in Figure 14 below. It may be seen that the highest truncation ratio R, close to 2.0, gives the best fit to the CAMILLE observation of Figure 9, which is the worst case of large scale breaking in about 3

hours of data. This frequency ratio of 2.0 is also the same as that used in the Draupner case in the previous Section. Figure 14 also establishes that particle escape is controlled by the single parameter significant steepness. We may conclude that a large breaking wave is to be expected about once per hour at the LILI significant steepness of 0.043, and about once per 100 hours at the IVAN significant steepness of 0.037.

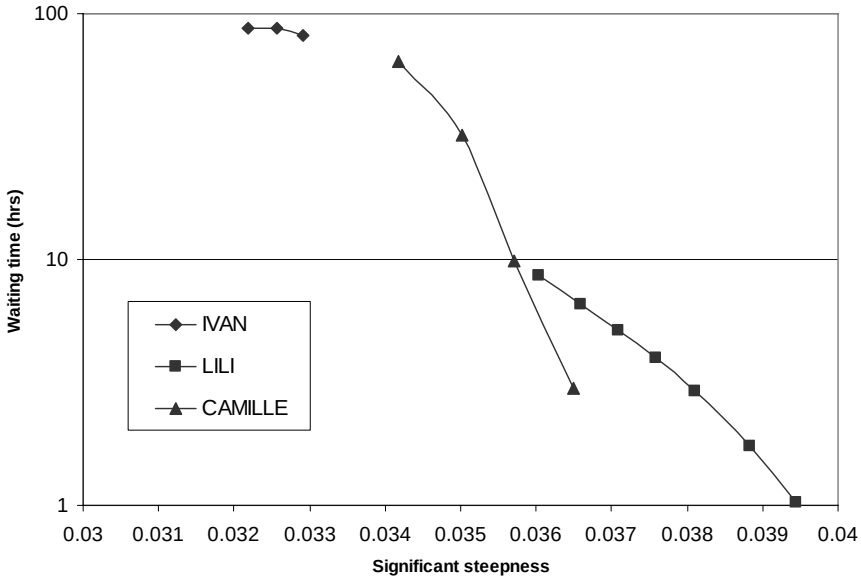

Figure 14. Waiting-times (in hours) until a particle escape, in the three hurricanes IVAN, LILI and CAMILLE, as a function of significant steepness. Several points are shown for each hurricane, corresponding to variously truncated spectra, of maximum-to-minimum frequency ratios between 1.5 and 2.0 (and including a value close to 2.0 in all three cases). The loss of significant waveheight produced by the truncation can be seen by comparing the significant steepness values with those for the original spectra shown in Figure 10, which were 0.037, 0.043 and 0.041 respectively.

This finding calls into question the mathematical models of large waves, such as those in the widely-used design code [52] for fixed steel offshore structures with small-diameter members. It is remarkable that none of the wave models in this code allow for breaking. As already noted after Figure 9, large breaking waves have much higher particle accelerations than non-breaking waves. Computations have shown [53] that where the water surface is vertical, the acceleration is typically 5g rather than at most 0.5*g*. This will produce, via the wave loading formulae for small-diameter members (which strictly speaking should be extended beyond the usual Morison form in these extreme condition [54, 55]) a much higher local wave load there, see e.g. [56]. It is also known that when the wave forces on fixed steel structures are measured by means of strain gauges, some waves appear to be more forceful than others, when compared with the predictions from non-breaking wave models [57].

Despite this evidence, [52] specifies that the water surface should be defined in the classical way as the sum of sinusoidal components (i.e. (1.1) with many frequency components), which clearly prevents any breaking. And that the velocity underneath this surface should be defined [52, para 2.3.1.c(2)] by modifying the classical velocity field (3.1) by means of "Wheeler stretching" [47] or a similar method. Much more sophisticated non-breaking wave models have been proposed, for example [58] is a method which does not allow a regular wave to break until $ka = 1$ [58, after fig.3]. It will thus give a non-breaking model of a breaking wave. It has also

been stated [51, sect.6(i)] that Stokes' expansion remains valid in the case of two combined waves of length ratio up to 2:1, provided it is valid for each wave individually. This is clearly incorrect (the exact computations in Figures 11 and 12 show that two waves of length ratio 2:1 will, when combined, break well before either would individually), and will lead the methods of [51] to produce a non-breaking model of a breaking wave.

It is hoped that the evidence of the breakdown of Stokes expansion, provided by particle escape, will encourage the use of more rigorous and realistic wave models. A modest step in that direction would be to include at least sharp-crested waves in the design code [52] cited above. A good model of a sharp-crested wave [59] has long been available, and is programmed into some commercial software. An alternative version, which is less elegant but conceptually simpler and even more accurate, has also recently been devised [60].

5. Conclusions

Recent evidence from field and laboratory data, and from computations, suggests that the weakly-nonlinear theory of water waves and wave-structure interaction (Stokes' expansion) may be less important than previously thought. In linear theory, the particles occasionally escape to infinity in finite time, and this appears to be associated with strongly-nonlinear behaviour, in which the surface can likewise be thrown upwards.

The explanation for the "ringing" of large-diameter vertical cylindrical members of offshore structures was once sought in weakly-nonlinear (3^{rd} order) theory, but it is now definitely known to be a strongly-nonlinear phenomenon. The water surface can be seen in high-speed photographs to behave in a violent fashion, as predicted to a remarkable degree by the movement of surface particles in linear theory.

The explanation for rogue waves, too, has long been sought in weakly-nonlinear theory (non-linear focusing by 3^{rd} order amplitude dispersion), but the latest computations based on that approach show that the effect is of negligible statistical significance, when set against the field observations (especially those in water too shallow to allow the Benjamin-Feir instability, which is the benchmark amplitude dispersion effect). Also laboratory experiments with focused waves show the crest elevation continuing to grow after all components have come into phase, which is inconsistent with weakly-nonlinear theory – but is exactly they type of strongly-nonlinear behaviour suggested by particle escape.

Computations are presented to establish the frequency of particle escape in the conditions of the well-known Draupner rogue wave, and the frequency (which is increased by the relatively shallow water at Draupner) is found to be consistent with the field observation. The implication of rogue waves being a strongly-nonlinear phenomenon of this type, is that they can be investigated by relatively simple laboratory experiments, because there is no need to allow the waves to evolve over great distances. Another important implication is that rogue waves may typically be associated with jets thrown upward from the wave crests. These have recently been seen in laboratory experiments in focused waves, and are readily observed at sea, in locally-extreme conditions. This offers an explanation for the elusive nature of rogue wave measurements, which are often discarded as "spurious crests due to spray".

Finally wave breaking itself has long been explained by weakly-nonlinear theory, as an unstable perturbation of regular waves. However, the latest theoretical investigations and computations show that the most relevant instability only produces breaking if the crest is close to the 120-degree limiting form, and then only on a small scale. It is known that in large-scale wave breaking the wave by-passes the 120-degree limiting form – it is this type of large-scale

wave breaking which appears to be better explained by particle escape.

Exact fully-nonlinear computations are presented of the simplest relevant case, which is two interacting waves of 2:1 length ratio, and the same steepness. The threshold steepness for wave breaking is found to correspond quite well with the threshold steepness for particle escape. For longer wave groups, the experimentally-observed threshold steepness for wave breaking also agrees well with the threshold steepness for particle escape. Computations are accordingly presented of the frequency of particle escape in the measured wave spectra of two recent hurricanes, LILI and IVAN, and one historical hurricane, CAMILLE, in which there is a measurement of large-scale breaking. By comparing the results, it is concluded that large-scale wave breaking will have occurred approximately once every hour, and once every 100 hours, in LILI and IVAN respectively.

These findings call into question the design codes for fixed offshore structures, which rely entirely on weakly-nonlinear theory – wave breaking is excluded. A revision to these codes would therefore appear to be timely. It could be based on simple models of sharp-crested waves which are already available commercial software.

Acknowledgments

I am indebted to Prof. D.H. Peregrine of Bristol University for the loan of his exact computer program, featured in Section 4. I am also indebted to the captain of the Cambridge University Canoe Club, Mr. P.J. Rainey, for the field observations cited above Figure 8. He has also kindly assisted his father by running Prof. Peregrine's program.

Appendix: Details of particle escape.

Particles on the diverging streamlines of Figure 2 move upwards increasingly rapidly. We can obtain the vertical velocity from (1.2), and so find their vertical position z, for large z, by solving the differential equation:

$$\frac{dz}{dt} = a\omega e^{kz} \tag{A1}$$

This equation integrates exactly (albeit that it is only valid for large z) to:

$$z = -k^{-1} \ln\{1 - ka\omega(t - t_0)\} \tag{A2}$$

where $z = 0$ at $t = t_0$. This expression becomes infinite when $ka\omega(t - t_0)$ reaches 1, in other words at the finite time:

$$t = t_0 + (ka\omega)^{-1} \tag{A4}$$

This event is known as a "blow-up" and is well-known in other contexts, for example combustion, see e.g. [61], and optics and plasma waves, see e.g. [62]

References

1. J. Grue (ed.), *Proc. 20th Int. Workshop on Water Waves and Floating Bodies.* London: R. Inst. Naval Architects (2005) (see www.rina.org.uk).
2. G.G. Stokes, On the theory of oscillatory waves. *Trans. Camb. Phil. Soc*. (1847). In *Mathematical & Physical Papers by G.G.Stokes*, Vol 1, (1880) 197-219. Cambridge University Press.
3. L.W. Schwartz, Computer extension and analytic continuation of Stokes' expansion for gravity waves. *J. Fluid Mech.* 62 (1974) 553-578.
4. S. Malenica and B. Molin, Third-harmonic wave diffraction by a vertical cylinder. *J. Fluid Mech.* 302 (1995) 203-229.
5. O.M. Faltinsen, J.N. Newman and T. Vinje, Nonlinear wave loads on a slender vertical cylinder. *J. Fluid Mech.* 289 (1995) 179-198.
6. J. Grue, G. Bjorshol and Ø. Strand, Higher harmonic wave exciting forces on a vertical cylinder. *Institute of Mathematics, University of Oslo Preprint*. No. 2. (1993) ISBN 82-553-0862-8 28 pp.
7. J.R. Chaplin, R.C.T. Rainey and R.W. Yemm, Ringing of a vertical cylinder in waves *J. Fluid Mech.* 350 (1997) 119-147.
8. R.C.T. Rainey and J.R. Chaplin, Wave breaking and cavitation around a vertical cylinder: experiments and linear theory. *Proc. 18th Int. Workshop on Water Waves and Floating Bodies.* (Ed. A.H. Clement & P. Ferrant). London: R. Inst. Naval Architects (2003) (see www.rina.org.uk).
9. T. Sarpkaya and M. Isaacson, *Mechanics of Wave Forces on Offshore Structures* New York: Van Nostrand Reinhold (1981) 651 pp.
10. T.B. Benjamin and J.E. Feir, The disintegration of wavetrains in deep water, Part 1, Theory. *J. Fluid Mech.* 27 (1967) 417-430.
11. C.C. Mei, *The applied dynamics of ocean surface waves,* Singapore: World Scientific (1989) 740pp.
12. D.H. Peregrine, Water waves, nonlinear Schrödinger equations and their solutions, *J. Australian Math. Soc.* B25 Pt 1 (1983) 16-43.
13. P.A.E.M. Janssen, Nonlinear four-wave interactions and freak waves *J. Physical Oceanography,* **33** (2003) 863-884.
14. H. Socquet-Juglard, K. Dysthe, K. Trulsen, H.E. Krogstad and J. Liu, Probability distributions of surface gravity waves during spectral change. *J. Fluid Mech.* 542 (2005) 195-216.
15. D.A.G. Walker, P.H. Taylor and R. Eatock Taylor, The shape of large surface waves on the open sea and the Draupner new year wave. *Applied Ocean Research* 26 (2005) 73-83.
16. P.A.E.M. Janssen and M. Onorato, The shallow water limit of the Zakharov equation and consequences for (freak) wave prediction. *Tech. Memorandum No. 464, European Centre for Medium-Range Weather Forecasts* (2005).
17. J. Skourup, N-E.O. Hansen, and K.K. Andreasen, Non-Gaussian Extreme Waves in the Central North Sea. *Trans. ASME,* 119, (1997) 146-150.
18. A. Ramamonjiarisoa and M. Coantic, Loi experimentale de dispersion des vagues produites par le vent sur une faible longueur d'action. *C.r.hebd Séanc Acad. Sci. Paris* B 282 (1976) 111-113.
19. J.R. Chaplin, On frequency-focusing unidirectional waves. *Int. J. Offshore & Polar Engng.* 6 No. 2 (1996) 131-137.
20. M.S. Longuet-Higgins and O.M. Phillips, Phase velocity effects in tertiary wave interactions. *J. Fluid Mech.* 12 (1962) 333-336.
21. J.A. Rice, *Mathematical statistics and data analysis* 2nd Ed. Belmont CA: Wadsworth Publishing Co. (1995).
22. M.L.Banner and D.H.Peregrine, Wave breaking in deep water. *Annu. Rev. Fluid Mech* 25 (1993) 373-397.
23. T. Waseda, Nonlinear wave generation in a tank (in Japanese) KANRIN J. Japan Soc. Naval Architects and Ocean Engineeers 4 (2006)
24. M.J. Sterndorff, and J. Gronbech, Short term probability distributions for extreme crest heights. *Proc. 19th Int. Conf. on Offshore Mechanics and Arctic Engng*. (2000) Trans ASME.

25. G.Z. Forristall, Wave crest distributions: observations and second-order theory. *J. Physical Oceanography* 30 (2000) 1931-1943
26. P. Stansell, Distributions of extreme wave, crest and trough heights measured in the North Sea. *Ocean Engineering* 32 (2005) 1015-1036
27. M.K. Ochi, *Ocean Waves – The Stochastic Approach.* Cambridge University Press (1998) 319 pp.
28. W.H. Buckley, Extreme waves for ship and offshore platform design: an overview. *Proc. 3rd Int. Conf. on Design and Operation for Abnormal Conditions.* London: R. Inst. Naval Architects (2005) (see www.rina.org.uk).
29. M.D. Earl, Extreme conditions during hurricane Camille. *J. Geophysical Research*. 80 no.3 (1975).
30. M.S. Longuet-Higgins, On wave breaking and the equilibrium spectrum of wind-generated waves. *Proc. R. Soc. Lond.* A310 (1969) 151-59.
31. M.S. Longuet-Higgins and M.J.H. Fox, Theory of the almost-highest wave: the inner solution. *J. Fluid Mech.* 80 (1977) 721-741.
32. R.C.T. Rainey, "Escape" of particle trajectories in linear irregular waves: a new explanation for wave breaking and model of breaking waves. *Proc. 17th Intl Workshop on Water Waves and Floating Bodies.* (Eds. R.C.T. Rainey and S.F. Lee) pp 155-158. London: R. Inst. Naval Architects (2002) (see www.rina.org.uk).
33. M.S. Longuet-Higgins and M. Tanaka, On the crest instabilities of steep surface waves. *J. Fluid. Mech.* 336 (1997) 51-68
34. M.S. Longuet-Higgins and D.G.Dommermuth, Crest instabilities of gravity waves. Part 3. Nonlinear development and breaking. *J. Fluid Mech.* 336 (1997) 33-50
35. M.S. Longuet-Higgins, On the overturning of gravity waves. *Proc. R. Soc. Lond.* A376 (1981) 377-400
36. J.W. Dold and D.H. Peregrine, An efficient boundary-integral method for steep unsteady water waves. *Numer. Meth. for Fluid Dynamics II* (Eds. K.W.Morton & M.J.Baines), Oxford University Press (1986). pp.671-679.
37. J.W. Dold, An efficient surface-integral algorithm applied to unsteady gravity waves. *J. Computational Physics*. 103 no.1 (1992), 90-115.
38. M.S. Longuet-Higgins and E.D. Cokelet, The deformation of steep surface waves on water. I. A numerical method of computation. *Proc. R. Soc. Lond.* A358 (1976) 1-26.
39. M.S. Longuet-Higgins and R.W. Stewart, Changes in the form of short gravity waves on long waves and tidal currents. *J. Fluid Mech.* 8 (1960) 565-583.
40. M.S. Longuet-Higgins and R.P. Cleaver. Crest instabilities of gravity waves. Part 1. The almost-highest wave. *J. Fluid Mech.* 258 (1994) 115-119.
41. E.O. Tuck, The effect of nonlinearity at the free surface on flow past a submerged cylinder *J. Fluid Mech.* 22 (1965) 401-404.
42. J.V. Wehausen, The wave resistance of ships. *Adv. Appl. Mech.* 13 (1973) 93-245.
43. H. Lamb, *Hydrodynamics*. 6th Ed. Cambridge University Press (1932) 738 pp.
44. F. Biesel, Study of wave propagation in water of gradually varying depth. *Gravity Waves*, U.S. National Bureau of Standards, Washington, Circular no. 521 (1952) 243-253.
45. F. Gerstner, Theorie der Wellen *Abh. d. k. Böhm. Ges. d. Wiss.* (1802) [Gilbert's *Annalen d. Physik,* xxxii (1809)].
46. S.H. Gjøsund, G. Moe and Ø.A. Arntsen, Kinematics in broad-banded irregular ocean waves by a Lagrangian formulation. *Proc. 20th Int. Conf. on Offshore Mech. and Arctic Engng. Conf.* (2001) 681 – 688. Trans. ASME.
47. J.D. Wheeler, Method of calculating forces produced by irregular waves, *Proc. Offshore Technology Conference* (OTC, Houston) (1970) 1, 71-82
48. P.J.H. Unna, "White horses" *Nature, Lond.* 148 (1941) 226-227.
49. O.M. Phillips, The dispersion of short wavelets in the presence of a dominant long wave, *J. Fluid Mech.* 107 (1981) 465-485.
50. M.S. Longuet-Higgins, The propagation of short surface waves on longer gravity waves, *J. Fluid Mech.* 177 (1987) 293-306.
51. J. Zhang, K. Hong and D.K.P. Yue, Effects of wavelength ratio on wave modelling, *J. Fluid Mech.* 248 (1993) 107-127.

52. American Petroleum Institute, *Recommended Practice for Planning, Designing and Constructing Fixed Offshore Platforms* (RP 2A-WSD) 21st Ed. (2000).
53. A.L. New, P. McIver and D.H. Peregrine, Computations of overturning waves, *J. Fluid Mech.* 150 (1985) 233-251.
54. R.C.T. Rainey, A new equation for calculating wave loads on offshore structures, *J. Fluid Mech.* 204 (1989) 295-324.
55. R.C.T Rainey, Slender-body expressions for the wave load on offshore structures, *Proc. R. Soc. Lond.* A450 (1995) 391-416.
56. R.C.T. Rainey, Breaking wave loads on immersed members of offshore structures. *HSE Rep.* OTH 89 311 (1989) London: HSE Books 28 pp.
57. J.C. Heideman and T.O. Weaver, Static wave force procedure for platform design. *Proc. 5th Int. Conf. on Civil Engineering in the Oceans.* (1992) College Station, Texas. American Society of Civil Engineers.
58. D.B. Creamer, F. Henyey, R. Schult and J. Wright, Improved linear representation of ocean surface waves. *J. Fluid Mech.* 205 (1989), 135-161.
59. M.S. Longuet-Higgins, On the form of the highest progressive and standing waves in deep water, *Proc. R. Soc. Lond.* A331 (1973) 445-456.
60. R.C.T. Rainey and M.S. Longuet-Higgins, A close one-term approximation to the highest Stokes wave on deep water, *Ocean Engineering* 33 (2006) 2012-2024.
61. J. Bebernes and D. Eberly, *Mathematical Problems from Combustion Theory* Springer Verlag (1989).
62. C. Sulem and P-L. Sulem, *The Nonlinear Schrodinger Equations: Self-focusing and Wave Collapse* New York: Springer Verlag (1999).